comes more clear when the change in the image defects are described as a function of β_0 under a constant value of α_0.

Fig. 18 illustrates the results. Only by the present instrument the image defects can be decreased with decreasing β_0.

Acknowledgement

The author wishes to express his thanks to Professor K. Ogata and Professor H. Matsuda for many helpful discussions and suggestions, to Dr. S. Kisaka, Manager of his Laboratory and Dr. C. Okazaki for their encouragement and to Mr. H. Tanaka for his programming of computer.

A New Mass Spectrograph with Very Large Dispersion

H. Matsuda, S. Fukumoto, and Y. Kuroda

Institute of Physics, College of General Education, Osaka University

and M. Nojiri

Japan Electron Optics Laboratory

(Z. Naturforschg. **21 a**, 25—33 [1966]; received 19 September 1965)

Dedicated to Prof. J. Mattauch *on his 70th birthday*

A new type of mass spectrograph with large mass dispersion has been constructed. The distinguishing feature of this apparatus is that the mass dispersing action of a r^{-1} magnetic field is utilized. The instrument has a r^{-1} magnetic field of 198.1° sector type (22 cm mean radius) as the dispersing field, a toroidal electric field of 118.7° sector type (30 cm mean radius) and a 30° uniform magnetic field (120 cm mean radius) as the focusing fields. The principle, the design and important parts of the apparatus are described. The dispersion on the photographic plate was estimated to be 14 cm for 1% mass difference and the maximum resolving power of about 500,000 was obtained.

A mass spectrograph with large mass dispersion and resolving power is useful for the precise determination of nuclidic masses. One method to obtain high resolution consists in enlarging the linear dimensions of the ordinary double focusing apparatus with cylindrical electric field and homogeneous magnetic field. During the past ten years, a number of large apparatus has been constructed [1], and a resolving power of several hundred thousand has been obtained. It seems, however, very difficult to enlarge the linear dimensions of the apparatus still more to increase the resolving power about one order of magnitude because of economic and technical reasons.

Another method for obtaining high resolution has been recently developed using a toroidal electric field and a non-uniform magnetic field [2]. Though this method is considered to be very promising, there might still be some technical difficulties in order to obtain a resolving power of several million.

About two years ago, one of the authors proposed a new method which might provide such high resolutions and mass dispersions without requiring very large linear dimensions [3]. It is the essential feature of this method to use a mass dispersing field which has no lens action. Since then, we were planning to construct a mass spectrograph which utilized this method. As a first step, in order to verify the principle experimentally and to study the characteristics of the dispersing field, we constructed a relatively small apparatus. The new mass spectrograph has a r^{-1} magnetic field as the dispersing field together with a toroidal electric field and a uniform magnetic field as the focusing fields.

[1] K. Ogata and H. Matsuda, Z. Naturforschg. **10 a**, 843 [1955]. — K. S. Quisenberry, T. T. Scolman, and A. O. Nier, Phys. Rev. **102**, 1071 [1956]. — C. Stevens, J. Terandy, G. Lobell, J. Wolfe, N. Beyer, and R. Lewis, Proc. Intern. Conf. Nuclidic Masses, University of Toronto Press, Toronto 1960, p. 403. — N. R. Isenor, R. C. Barber, and H. E. Duckworth, ibid., p. 439. — K. T. Bainbridge and P. E. Moreland, Jr., ibid., p. 460. — H. Hintenberger, J. Mattauch, H. Wende, H. Voshage, and W. Müller-Warmuth, Advan. Mass Spectr. **2**, 180 [1963]. — H. Ewald, E. Konecny, H. Opower, and H. Rösler, Z. Naturforschg. **19 a**, 194 [1964].

[2] H. W. Wachsmuth and H. Ewald, Z. Naturforschg. **18 a**, 389 [1963].

[3] H. Matsuda, Mass Spectroscopy (Japan) **11**, 127 [1964].

Principle

The distinguishing feature of the apparatus is the use of the prismatic action of the dispersing field. Therefore, we shall describe the characteristic of the dispersing field briefly, the details have been reported previously [3].

In the first place, we consider the ion orbit in the median plane of the sector type field (electric or magnetic), whose field strength is given as follows:

$$E_r = E_0(1 + l\varrho + \ldots): \quad \text{electric}, \tag{1}$$

$$H_z = H_0(1 + n\varrho + \ldots): \quad \text{magnetic}. \tag{2}$$

Here, we use the cylindrical coordinate system (r, φ, z) and put $r = a(1+\varrho)$, $(\varrho \ll 1)$, where a is the radius of the central beam. In case of $l = -3$ or $n = -1$, the differential equation which gives the ion orbit in the first order approximation becomes

$$d^2\varrho/d\varphi^2 = \delta', \tag{3}$$

$$\delta' = \gamma + 2\beta: \quad \text{electric}, \tag{4}$$

$$= \gamma + \beta \ : \quad \text{magnetic}, \tag{5}$$

where γ and β are fractions of mass and velocity respectively. The solution is given by:

$$\varrho = \alpha_r'\varphi + \tfrac{1}{2}\delta'\varphi^2 + \varrho_1, \tag{6}$$

$$d\varrho/d\varphi = \alpha_r' + \delta'\varphi, \tag{7}$$

α_r' being the incident angle of the ion beam. These equations show that the electric field with $l = -3$ or the magnetic field with $n = -1$ has no focusing (lens) action but dispersive (prismatic) action in the first order approximation. If parallel ion beams (including ions with various δ' values) are injected into such a field, then ions with the same δ' value will remain still parallel to each other but ions with different δ' values will have different directions after passing through the field. We call such a field a dispersing field. The dispersive action of the field is analogous to the optical prism.

The ordinary sector type field, used as a particle analyzer, has the focusing and dispersive actions simultaneously. If it is divided in two at the point where the ion beams become parallel, then the source and the image are located at the respective focal points of the divided sector fields. Let the deflecting angle of each field be Φ_1 and Φ_3 as shown in Fig. 1 (b), then the focal lengths f_1 and f_3 are given by the following equations:

$$f_1 = \frac{a}{\varkappa}\,\frac{1}{\sin \varkappa \Phi_1}, \tag{8}$$

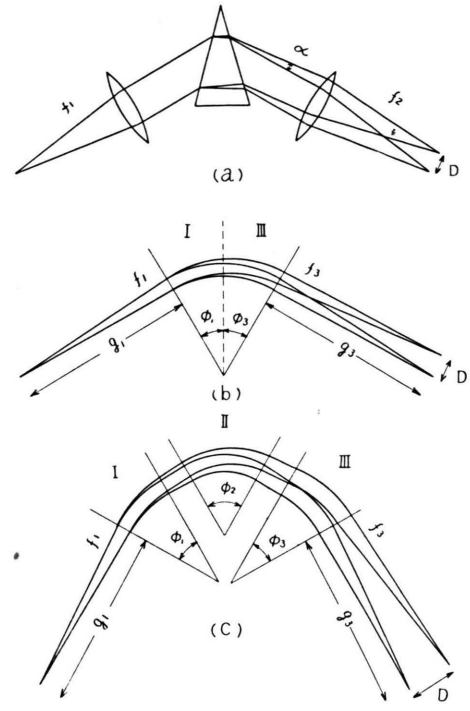

Fig. 1. Schematic diagrams which show the principle of the new mass spectrograph with dispersing field.

(a) Optical prism spectrograph, $D = f_3\,\alpha$.

(b) Ordinary mass spectrograph, $D = \left(\frac{a}{\varkappa^2 f_1} + \frac{a}{\varkappa^2 f_3}\right) f_3\,\delta'$.

(c) Mass spectrograph with dispersing field,
$D = \left(\frac{a}{\varkappa^2 f_1} + \frac{a}{\varkappa^2 f_3} + \Phi_2\right) f_3\,\delta'$.

$$f_3 = \frac{a}{\varkappa}\,\frac{1}{\sin \varkappa \Phi_3}, \tag{9}$$

where a is the mean radius and $\varkappa$ the field characterizing constant. The dispersion D at the image is given by

$$D = \left(\frac{a}{\varkappa^2 f_1} + \frac{a}{\varkappa^2 f_3}\right) f_3\,\delta', \tag{10}$$

and the magnification by f_3/f_1. Therefore, if the slit width of the source is taken to be s, the resolving power R is given by

$$R = \left(\frac{a}{\varkappa^2 f_1} + \frac{a}{\varkappa^2 f_3}\right)\frac{f_1}{s}. \tag{11}$$

Now, suppose we separate these two fields and insert a dispersing field in between as shown in Fig. 1 (c), the deflecting angle being Φ_2. This arrangement of the fields is quite analogous to the optical prism spectrograph shown in Fig. 1 (a). Separated fields act as focusing lenses. We shall call them the focusing fields.

The dispersive field has no lens action, as mentioned above. Therefore the locations of source and image will not change. The dispersion is given by

$$D=\left(\frac{a}{\varkappa^2 f_1}+\frac{a}{\varkappa^2 f_3}+\Phi_2\right) f_3\,\delta'. \qquad (12)$$

Comparing equations (10) and (12) it is seen that the dispersion increases by $\Phi_2 f_3 \delta'$ in the latter case. Since the magnification does not change, the resolving power of the analyzer will increase by $\Phi_2 f_1/s$.

If f_1 and f_3 are very large, both dispersion and resolving power increase very much compared with the ordinary case. For example, if the separated fields are homogeneous magnetic fields with $\Phi_1=\Phi_3=30^\circ$, and the inserted field is a magnetic dispersing field with $\Phi_2=180^\circ=\pi$, then an about fourfold increase in both dispersion and resolution is expected. Nevertheless, the total size of the whole apparatus will not become so large, because the radius of the dispersing field can be kept much smaller than the radius of the focusing field, for the dispersive action does not depend on its radius.

In the case of a magnetic analyzer, the dispersing field is the magnetic field. The strength of it varies proprotional to r^{-1}. Such a field is easily realized in the region between the conical pole faces, and the condition for the dispersing field holds everywhere between the pole faces independent of radius. This feature of the field is quite satisfactory for practical application.

Design

In order to get high resolving power for a mass spectrograph, the apparatus must be a double focusing one with electric and magnetic fields. Therefore, let the first focusing field be an electric field, and the dispersing field and the second focusing field be magnetic fields. The deflection in the electric field and that in the magnetic fields should be in opposite directions. A toroidal electric field is suitable as the first field because the velocity dispersing angle which must be compensated is very large. For the second focusing field, a homogeneous magnetic field is preferable for technical reasons.

In this arangement of the three fields, the double focusing condition in the first order approximation is given by [3]:

$$(2/\varkappa_e)\sin\varkappa_e\Phi_e=\sin\Phi_{m3}+\Phi_{m2}, \qquad (13)$$

where suffices e and m indicate electric and magnetic fields respectively. When this double focusing condition is satisfied, the mass dispersion at the image point is given by

$$D_m=\tfrac{1}{2}(a_{m3}+f_{m3}\Phi_{m2})\,\gamma, \qquad (14)$$

and the resolving power by

$$R=a_e/(\varkappa_e^2 s). \qquad (15)$$

Though the r^{-1} magnetic field has no lens action upon the motion of the ions in the r-direction, it has a focusing effect on the motion in the z-direction, the field characterizing constant $\varkappa_z$ being 1. In order to get higher mass dispersion, it is desirable to make the deflecting angle Φ_{m2} as large as possible. But, considering the focusing action in the z-direction, this angle was chosen to be $\Phi_{m2}=198.1^\circ=3.457$.

The values of Φ_{m3} and $\varkappa_e\Phi_e$ were both chosen to be 30° in order to make the focal lengths large. Then, the value of $\varkappa_e$ is calculated to be 0.2527 from the double focusing condition (13). Since $\varkappa_e\Phi_e$ was chosen to be 30°, Φ_e becomes 118.7°. The radii of the three fields were chosen to be $a_e=30$ cm, $a_{m2}=22$ cm and $a_{m3}=120$ cm by considering the size of the electrodes and the magnets. The distance between two successive fields may be chosen arbitrarily, and the following values were adopted for practical convenience in the design of a vacuum chamber: $\Delta_1=22$ cm and $\Delta_2=24$ cm.

The source and the image are located at the focal points of the focusing fields. Therefore, the distance between the source and the first field, l', and that between the image and the third field, l'', are calculated from the following equations:

$$l'=g_e=(a_e/\varkappa_e)\cot\varkappa_e\Phi_e, \qquad (16)$$

$$l''=g_{m3}=a_{m3}\cot\Phi_{m3}. \qquad (17)$$

From these equations, the values of 205.6 cm for l' and 207.8 cm for l'' are obtained.

The schematic diagram of the ion path is shown in Fig. 2 (a). The image point for the z-directional focusing is located at $l_z''=430$ cm in this arrangement. The reason for locating this point so far away from the r-directional image point is to prevent a decrease in resoluiton caused by the ion beam outside the median plane. The mass dispersion perpendicular to the ion beam is calculated to be $475\,\gamma$ cm and the magnification of the image to be 1.01. If the width of the source slit is taken to be 0.005 mm, a maximum resolution of 940,000 may be expected.

Φ_e	118.7°	Δ_1	22 cm
a_e	30 cm	Δ_2	24 cm
$\varkappa_e$	0.2527		
$l' = g_e$	205.6 cm	dR_e/dr_e	0.237
f_e	237.4 cm	a_{m2}/k'	1.124
Φ_{m2}	198.1°	a_{m2}/k''	−0.178
a_{m2}	22 cm	a_e/q'	3.41
n	−1		
Φ_{m3}	30°	l_z''	430 cm
a_{m3}	120 cm		
$l'' = g_{m3}$	207.8 cm	Dispersion	475 γcm
f_{m3}	240 cm	Magnification	1.01

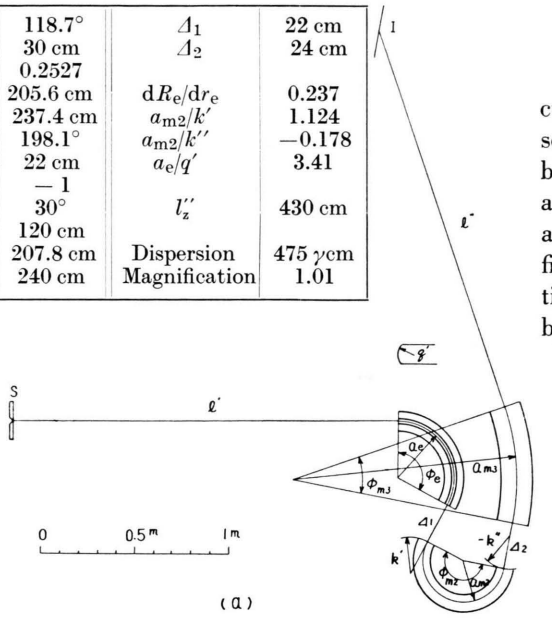

Fig. 2. (a) Schematic diagram of the ion path.

1	Ion source	11	Pole piece (uniform)
2	Focusing electrodes	12	Exciting coil
3	Shutter	13	Photographic plate
4	Horizontal slit	14	Faraday cage
5	Objective slit	15	Straight valve
6	Monitor	16	Ionization Gauge
7	α defining slit	17	Liquid-N_2 Trap
8	β defining slit	18	Oil diffusion pump
9	Toroidal condenser	19	Mechanical pump
10	Pole piece (r^{-1})	20	Ion getter pump

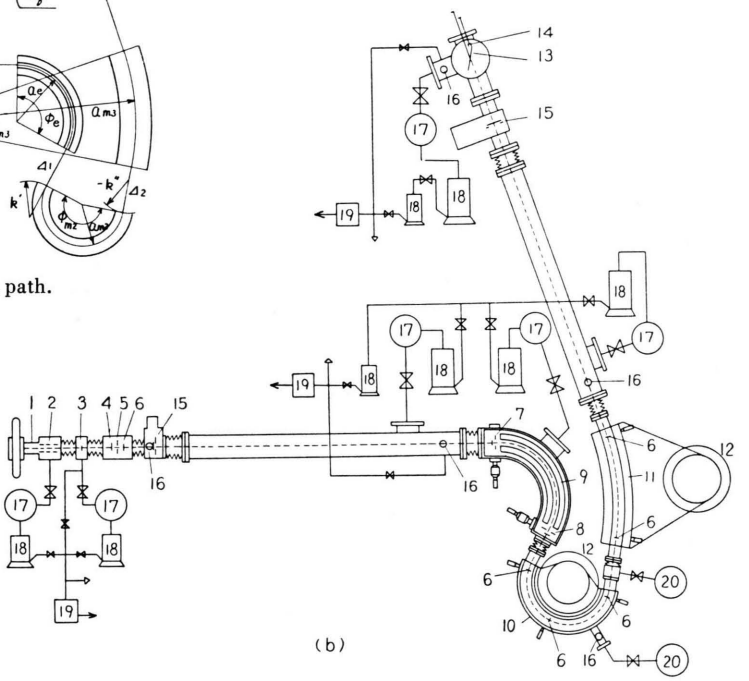

Fig. 2. (b) Schematic drawing of the mass spectrograph.

Second Order Consideration

The second order ion trajectories should be calculated in order to estimate the image defect. The second order ion path in a toroidal electric field has been calculated by EWALD and LIEBL [4], and that in a uniform magnetic field by HINTENBERGER, WENDE and KÖNIG [5]. Here, the ion path in the r^{-1} magnetic field is calculated in the second order approximation. The ion path behind the field may be expressed by the following equation:

$$\begin{aligned} y'' = a(&D_1\alpha_r' + D_2\beta + D_4\varrho_1 + D_{11}\alpha_r'^2 + D_{22}\beta^2 + D_{33}\alpha_z'^2 + D_{44}\varrho_1^2 + D_{55}\zeta_1^2 + D_{12}\alpha_r'\beta + D_{14}\alpha_r'\varrho_1 \\ &+ D_{24}\varrho_1\beta + D_{35}\alpha_z'\zeta_1) + x''(E_1\alpha_r' + E_2\beta + E_4\varrho_1 + E_{11}\alpha_r'^2 + E_{22}\beta^2 + E_{33}\alpha_z'^2 \\ &+ E_{44}\varrho_1^2 + E_{55}\zeta_1^2 + E_{12}\alpha_r'\beta + E_{14}\alpha_r'\varrho_1 + E_{24}\varrho_1\beta + E_{35}\alpha_z'\zeta_1). \end{aligned} \tag{18}$$

In case of normal incidence and exit at curved boundaries, the coefficients, D_i, E_i, may be written as:

$$\begin{aligned} &D_1 = \Phi, \quad D_2 = \tfrac{1}{2}\Phi^2, \quad D_4 = 1, \\ &D_{11} = \tfrac{1}{4}\Phi^2, \quad D_{22} = \tfrac{1}{12}\Phi^4 - \tfrac{1}{2}\Phi^2, \\ &D_{33} = -\tfrac{1}{8}(1-\cos 2\Phi), \\ &D_{44} = \tfrac{1}{2}(a/k')\Phi, \quad D_{55} = \tfrac{1}{8}(1-\cos 2\Phi), \\ &D_{12} = \tfrac{1}{3}\Phi^3, \quad D_{14} = \Phi, \\ &D_{24} = \tfrac{1}{2}\Phi^2, \quad D_{35} = \tfrac{1}{4}(2\Phi - \sin 2\Phi), \\ &E_1 = 1, \quad E_2 = \Phi, \quad E_4 = 0, \end{aligned} \tag{19}$$

$$\begin{aligned} &E_{11} = \tfrac{1}{2}(a/k'')\Phi^2 - \tfrac{1}{2}\Phi, \\ &E_{22} = \tfrac{1}{8}(a/k'')\Phi^4 - \tfrac{1}{6}\Phi^3 - \Phi, \\ &E_{33} = -\tfrac{1}{4}\sin 2\Phi, \\ &E_{44} = \tfrac{1}{2}a[(1/k') + (1/k'')], \quad E_{55} = \tfrac{1}{4}\sin 2\Phi, \\ &E_{12} = \tfrac{1}{2}(a/k'')\Phi^3 - \tfrac{1}{2}\Phi^2, \quad E_{14} = (a/k'')\Phi, \\ &E_{24} = \tfrac{1}{2}(a/k'')\Phi^2, \quad E_{35} = \tfrac{1}{2}(1-\cos 2\Phi), \end{aligned}$$

where α_r' and α_z' are initial angular divergences in r- and z-direction respectively, and Φ the deflecting angle. k' and k'' are the radii of the curvature of the boundaries at the entrance and the exit respectively.

[4] H. EWALD and H. LIEBL, Z. Naturforschg. **12 a**, 28 [1957].

[5] H. HINTENBERGER, H. WENDE, and L. A. KÖNIG, Z. Naturforschg. **10 a**, 605 [1955].

The image width at the position of the final focus can be calculated by combining the above three results. The expression for negligible small slit width has the form:

$$y_B = a_{m3}(B_{11}\,\alpha_r^2 + B_{12}\,\alpha_r\,\beta + B_{22}\,\beta^2 + B_{33}\,\alpha_z^2), \quad (20)$$

where α_r and α_z are radial and axial angles of divergence of the ion beam on the entrance side. The coefficients of the second order aberration, B_{11}, B_{12}, B_{22}, are expressed as functions of three parameters, R_e', k' and k''. R_e' is the derivative of the radius of curvature, R_e, of the equipotential line in the $r-z$ plane of the toroidal electric field [4], and is given by

$$R_e' = (\mathrm{d}R_e/\mathrm{d}r)_{r=a_e,\, z=0}\,. \quad (21)$$

Consequently, it may be possible to make $B_{11} = B_{12} = B_{22} = 0$ by choosing suitable values for R_e', k' and k''. In our case, these values are calculated to be

$$R_e' = 0.273\,,$$
$$a_{m2}/k' = 1.124\,,$$
$$a_{m2}/k'' = -0.178\,.$$

The remaining coefficient B_{33} can be made zero if the front faces of the electrodes of the toroidal condenser are made cylindrically curved [6]. The condition for $B_{33} = 0$ is satisfied if we take the value

$$a_e/q' = 3.41\,,$$

where q' is the radius of curvature in the $x'-z$ plane at the entrance of the condenser electrodes.

The inclination of the image curve against the focusing beam is also calculated from the second order consideration [7]. The angle between the direction of the focusing ion beam and the image curve at the double focusing point is calculated to be about 24° for directional focusing and 17° for velocity focusing.

The conditions for the second order focusing are shown in Fig. 1 (a) schematically.

Apparatus

The schematic drawing of the mass spectrograph constructed is shown in Fig. 2 (b), and Fig. 3 gives a general view. Following, the important parts of the apparatus are described briefly.

(1) Ion source

Ions, formed in an insulated metal housing kept at high voltage, are accelerated through an orifice of 2 mm ϕ and focused on the main slit by means of a focusing lens system. The lens system consists of three cylindrical electrodes made of stainless steel. The first and the third cylinders are accelerating electrodes and are grounded. The second is the decelerating one and the focal length of the lens system is controlled by changing the potential applied to it. The direction of the collimated ion beam can be adjusted mechanically. In a preliminary test, potassium ions from hot tungsten ribbon were accelerated with a voltage of about 15 kV which was regulated with a stability of less than 1/2000.

(2) Main slit system

The main slit is made out of two stainless steel plates of 1 mm thickness which are fixed on the rotatable slit holder with a gap of about 0.08 mm. The effective width of the slit can be adjusted by rotating it around the vertical axis at the center of the slit [8]. In front of the main slit, there is a horizontal slit of 0.5 mm width, the vertical position of which is adjustable. Behind the main slit, there is a monitor electrode which can be inserted if necessary. The ion current through the main slit can be measured by this monitor in order to estimate the effective slit width. A shutter for the ion beam is inserted between the collimating lens system and the main slit system.

(3) Energy selector

The energy selector consists of the toroidal condenser, the auxiliary electrodes, the α- and β-defining slits, and the vacuum chamber which encloses these assemblies. All are made of 18 − 8 stainless steel. The cross section is shown in Fig. 4.

The toroidal electric field of this apparatus should have the following parameters:

$$\Phi_e = 118.7°, \quad \varkappa_e = 0.2527, \quad a_e = 30\text{ cm},$$
$$R_e' = 0.237, \quad a_e/q' = 3.41.$$

The dimensions of the condenser electrodes which produce such a field are calculated by means of the method given by Liebl and Ewald [9]. The dimensions of electrodes actually made were measured with an accuracy of about 0.1 mm. They are:

$$r_a = 309.1\text{ mm}, \qquad r_b = 290.5\text{ mm},$$
$$R_a = 157.1\text{ mm}, \qquad R_b = 152.7\text{ mm},$$

where the notations are those used by Liebl and Ewald [9]. Under these conditions, the field between the electrodes is estimated to have the desired value within an accuracy of 0.2%. The Herzog end plates are used at the entrance and the exit of the condenser, the effective boundaries being supposed to be at the ends of the electrodes [10]. At the entrance, the face of the electrodes and the Herzog end plate are cylindrically curved, the value of q' being 88 mm.

[6] H. Liebl and H. Ewald, Z. Naturforschg. **12 a**, 541 [1957].
[7] H. Liebl, Optik **16**, 19 [1959].
[8] H. Ewald, Z. Naturforschg. **5 a**, 229 [1950].
[9] H. Liebl and H. Ewald, Z. Naturforschg. **14 a**, 842 [1959].
[10] R. Herzog, Phys. Z. **41**, 18 [1940].

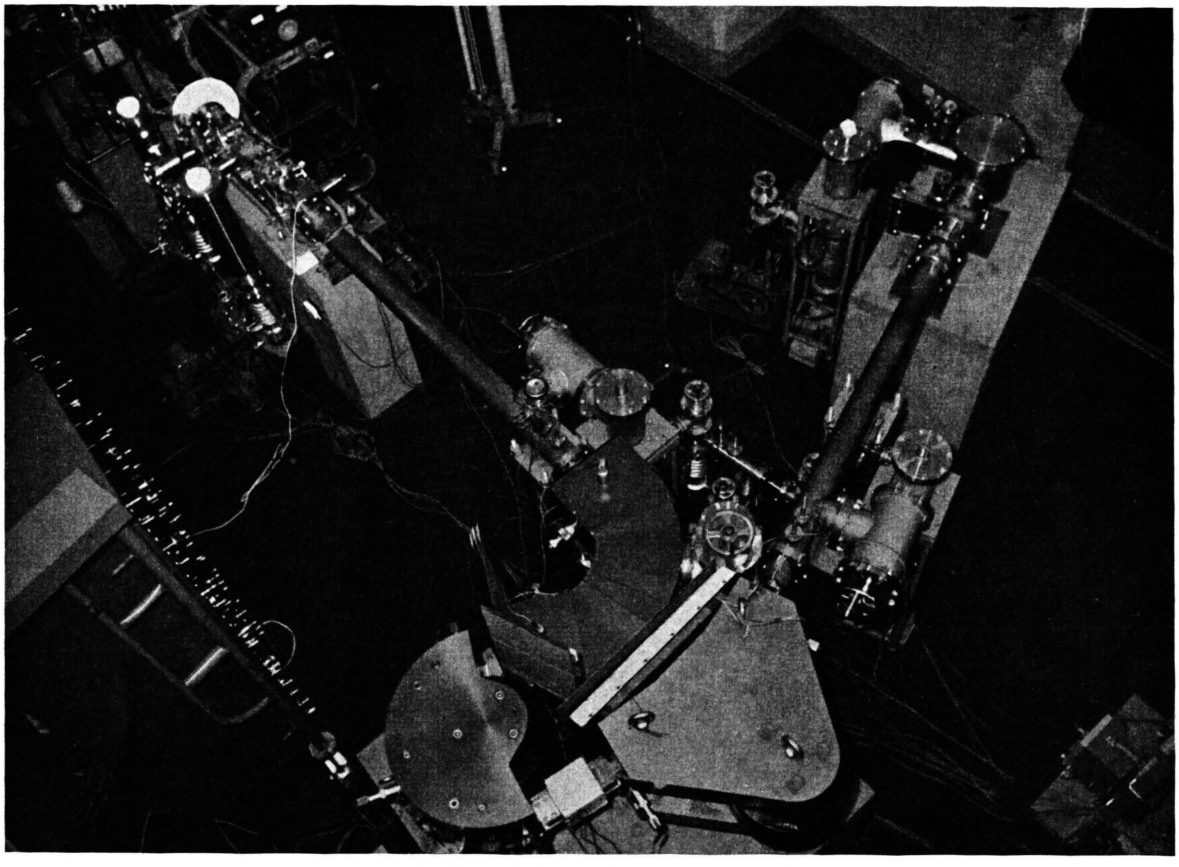

Fig. 3. General view of the mass spectrograph.

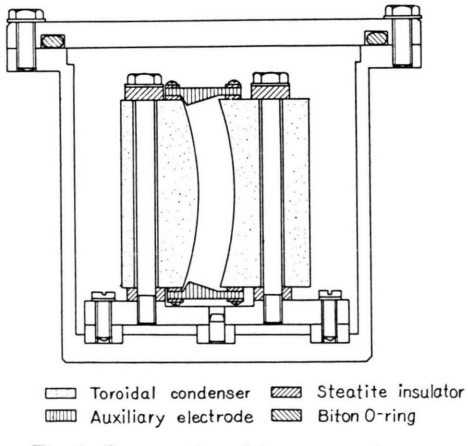

Fig. 4. Cross section of the energy selector.

Two auxiliary electrodes are placed above and below the gap of the toroidal electrodes. By applying suitable potentials to them, the field shape near the center may be finely adjusted [11]. The α- and β-defining slits are placed about 3 cm outside the HERZOG plates. The lateral position and the width of the slit can be adjusted from outside the chamber.

[11] H. MATSUDA, Rev. Sci. Instr. **32**, 850 [1961].

(4) Dispersing magnet

The dispersing magnet is a 198.1° sector type magnet with 22 cm mean radius. The cross section is shown

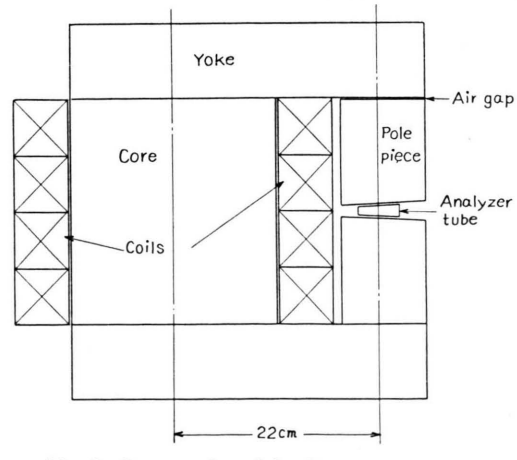

Fig. 5. Cross section of the dispersing magnet.

in Fig. 5. The pole pieces are made of soft iron with a carbon content of 0.03%, and have conical pole faces. By means of four distant wedge-shaped pieces of phosphor bronze, the pole gap is adjusted so that the vertices of the circular cones of the upper and the lower pole faces are brought exactly to the same point. The pole gap is 15 mm at the mean radius. In order to adjust the pole gap, there is an air gap of 0.5 mm between the upper pole piece and the yoke plate.

The HERZOG iron shields are attached to the entrance and the exit of the pole pieces. The location of them and the measured field distribution are shown in Fig. 6. From this distribution curve, the effective boundary of the field is estimated to be 5.5 mm outside of the pole edge. This agrees well with the expected value given by HERZOG [10]. The boundaries of the pole pieces and the HERZOG iron shield are curved so that the curvature of the effective boundary is expected to have the desired values: $k' = 195.5$ mm, $k'' = -1237$ mm.

The analyzer vacuum tube is made of SUS-33 stainless steel in order to reduce magnetizing effects. The cross section is shown in Fig. 5. The monitor electrodes can be inserted at three different points along the ion path in order to know where the actual beam travels.

There are four exciting coils having 12,100 turns each, wound with 0.45 mm ϕ copper wire. The total weight of the dispersing magnet is about 400 kg.

(5) Focusing magnet

The focusing magnet is a 30° sector type magnet with parallel pole faces. The mean radius is 120 cm and the pole gap 15 mm. The HERZOG iron shields, similar to the shields of the dispersing field, are attached to the entrance and the exit. Two exciting coils are used having 12,330 turns each. The total weight of the focusing magnet is about 540 kg.

(6) Camera

There are a plate holder and a FARADAY cage in the camera chamber. The size of the photographic plate is 45×150 mm^2. The plate holder can be shifted vertically for taking five series of mass spectra. A detecting slit is placed at the top of the plate holder. By setting the detecting slit into the beam plane, the mass spectrum can be detected electrically. The angle between the direction of the focusing beam and the photographic plate is adjustable.

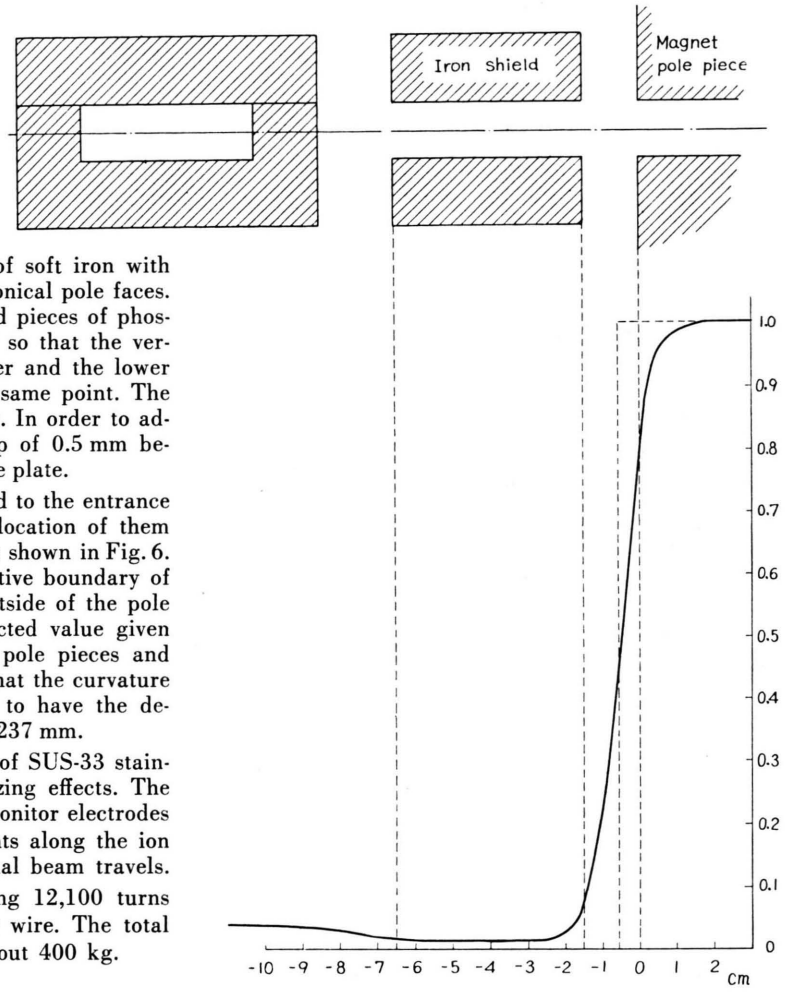

Fig. 6. HERZOG iron shield and fringing field distribution.

Stray Magnetic Field

It is very important to reduce the stray magnetic field as much as possible in order to realize a good focusing condition. The distribution of the stray field along the ion path was measured after setting the dispersing magnet and the focusing magnet at the calculated position. During these measurements, the field strength of the dispersing magnetic field was kept at 4,090 gauss and that of the focusing field at 750 gauss. These field strengths are nearly the same as under the operating conditions.

As an example of the results, the stray field distribution toward the electric field is shown in Fig. 7. Curve 1 shows the case with no magnetic shielding except the HERZOG iron shield where a considerable amount of stray field can be seen. When the energy selector is covered with Si steel sheets, the stray field is reduced as shown by curve 2, but the shielding effect

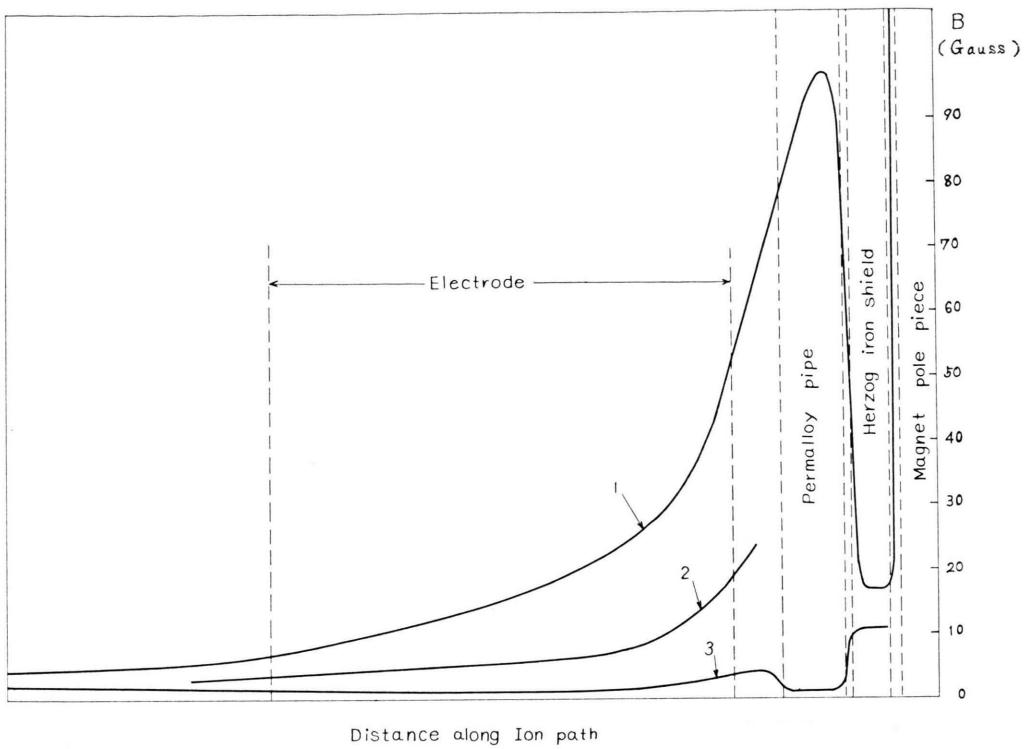

Fig. 7. Effect of shielding on stray magnetic field. 1 With HERZOG ion shield only, 2 Energy selector is shielded with Si steel sheets. 3 Permalloy pipe and iron sheets are inserted additionally.

is not yet satisfactory. A considerable improvement was attained by inserting a permalloy pipe and laminated iron sheets between the energy selector and the magnets. The final result is shown by curve 3.

Under the final condition of the magnetic shielding, the total deflection of the beam due to stray magnetic field may be estimated to be less than 1/1000 of the total deflection in the magnetic fields.

Preliminary Results

As a preliminary test, $^{39}K^{+}$ thermal ions accelerated to about 14.5 keV were used. The vacuum during the experiment is estimated to be 1×10^{-6} mm Hg in the energy selector, 4×10^{-6} mm Hg in the dispersing magnetic field, and 4×10^{-7} mm Hg at the exit of the focusing magnetic field, as measured by ionization gauges.

The potential between the electrodes of the toroidal condenser is about 1776 volts and is supplied from the layer dry batteries grounded at the center. Two auxiliary electrodes are grounded in this experiment. The exciting current for the dispersing magnet is finely adjusted so that the ion beam passes along the calculated orbit. The beam position in the magnetic field can be traced by means of the monitor electrodes which can be inserted at three different points along the ion path. The exciting current for the focusing magnet is adjusted so that the ion current is detected by the FARADAY cage in a camera chamber.

When exposures are made, the potentials applied to the condenser electrodes and also the accelerating voltages are slightly shifted for each successive exposure while keeping the magnetic fields constant, so that nine spectral lines are photographed in one exposure series. The mass dispersion on the photographic plate may be estimated from the potential values corresponding to respective spectral lines. An example of the photograph thus obtained is shown in Fig. 8. The potential shifted between successive exposures is about 1.1 volts and the potential of the center line 1776 volts.

From these values and the distances between spectral lines, the mass dispersion on the photographic plate is estimated to be about 14 mm for 0.1% mass difference. The angle between the photographic plate

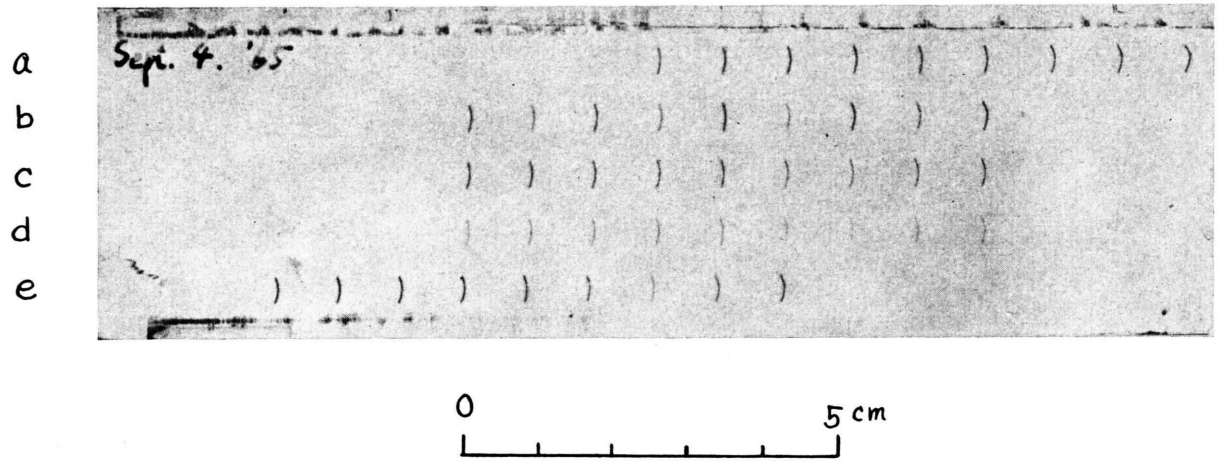

	a	b	c	d	e
Dispersing magnet current (mA)	683	683	683	683	683
Focusing magnet current (mA)	100	101	101	101	102
α-defining slit (mm)	1	1	0.3	0.3	0.3
β-defining slit (mm)	1	1	0.3	0.3	0.3
Exposure time (sec)	1	1, 0.3	3	1	2

Fig. 8. Example of mass spectra. $^{39}K^{+}$ lines are shifted by changing the potential between condenser electrodes. The shifted potential between successive exposures is 1.1 volts and the potential of center line 1776 volts. The width of main slit is 0.008 mm.

and the direction of the ion beam was about 21°, so the dispersion agrees well with the calculated value. The resolving power is estimated to be about 500,000 for the sharpest spectral line, photographed under the following conditions: the width of main slit, 0.008 mm; α-defining slit, 0.3 mm; β-defining slit, 0.3 mm; exposure time, 1 sec. These slit widths correspond to the values,

$$\alpha_{max} = 1/10{,}000, \qquad \beta_{max} = 2.5/10{,}000 .$$

The spectral lines are considerably curved as can be seen from Fig. 8. The cause why they are curved is not yet clear. We are now trying to obtain straight sharper lines in order to get higher resolution.

The authors wish to express their sincere thanks to Prof. K. Ogata and Prof. N. Sasaki for their valuable discussions, to Prof. T. Nagamiya and Prof. T. Watanabe for their encouragement, to Prof. Y. Asano and other members of the Institute and to Nishina Kinen Zaidan for their financial support, and to Mr. Y. Wada, Dr. T. Takeshita and Dr. S. Kobiyama for their kind support.

This work has been partly supported by the Scientific Research Found of the Ministry of Education.